Molecular Interaction of Cytotoxic Anticancer Analogues as Inhibitors of β-tubulin Protein Against UACC-62 Melanoma Cell

Kuan-Chung Chen
School of Pharmacy, China Medical University, Taichung, 40402, Taiwan
Chi-Rei Wu
Department of Chinese Pharmaceutical Sciences and. Chinese Medicine Resources, China Medical University, Taichung, 40402, Taiwan
Jin-Cherng Lien (jclien@mail.cmu.edu.tw)
School of Pharmacy, China Medical University, Taichung, 40402, Taiwan https://orcid.org/0000-0002-1211-0245

Research article

Keywords: β-tubulin, Molecular docking simulation, Pharmacophore features, Quantitative structure–activity relationship (QSAR) models

Posted Date: August 4th, 2020

DOI: https://doi.org/10.21203/rs.3.rs-49245/v1

Version of Record: A version of this preprint was published at The Journal of Biochemistry on January 21st, 2021. See the published version at https://doi.org/10.1093/jb/mvaa149.

Abstract

Background

In previous research, a series of cytotoxic anticancer analogues related to 2-acylamino-1,4-naphthoquinone derivatives has been demonstrated. As microtubule plays an important role in many essential cellular processes such as mitosis, tubulin is an important target of anticancer drug.

Methods

This study performed molecular docking simulation, pharmacophore model, comparative force field analysis model, and comparative similarity indices analysis model to investigate the relationship between inhibitory activities and the properties of compounds, in order to further progress the development of cytotoxic anticancer analogues.

Results

These compounds have common H-bond interactions with key residues Lys254 and Lys352, but compounds with large R^2 substituent have different docking poses than compounds with small R^2 substituent. Some of derivatives such as compound **18** formed the H-bonds with residue Lys254 using the oxygen atoms in R^1 substituent and formed π-cation interactions with residue Lys352 using phenyl moiety of 1,4-naphthoquinone. The R^1 substituent of these compounds preferred to have disfavored hydrophobic fields and favorable space toward the direction of residue Asn258, while the R^2 substituent of these compounds preferred to have about 2–3 carbon chain length hydrophobic substituent toward the direction of residues Ala316 and Lys352.

Conclusion

These results offer some beneficial advices for further study in anticancer drug development process.

Author Summary

A series of cytotoxic anticancer analogues related to 2-acylamino-1,4-naphthoquinone derivatives has been identified in previous research. In this study, we perform the molecular docking simulation for *β*-tubulin protein with these anticancer analogues to identify their possible docking poses. For quantitative structure–activity relationship models study, we also performed pharmacophore model to investigate the common pharmacophore features and performed comparative force field analysis, and comparative similarity indices analysis models to investigate relationship between inhibitory activities and their five physico-chemical properties. According to the results above, we can offer some beneficial advice for

further study in development process of designing of lead compounds with improved anticancer bioactivity.

Introduction

In previous research, it demonstrates a series of cytotoxic anticancer analogues related to 2-acylamino-1,4-naphthoquinone derivatives with their inhibitory concentration (1). Microtubules, which are polymerized by α-tubulins and *β*-tubulins, are a major component of the cellular cytoskeleton (2, 3). It is a major cellular target of anticancer drug as it plays an important role in many essential cellular processes such as mitosis (4–7). Tubulin-binding drugs kill tumor cells by inhibiting microtubule dynamics required in cell division (8–10). In this study, we performed molecular docking simulation to identify binding conformations and interactions between compounds and *β*-tubulin protein, in order to investigate the protein-ligand interaction network responsible for their anticancer activities. For quantitative structure–activity relationship (QSAR) models study, we also performed pharmacophore model to investigate the common pharmacophore features, and we performed comparative force field analysis (CoMFA) and comparative similarity indices analysis (CoMSIA) models to investigate relationship between inhibitory activities and their five physico-chemical properties in order to further progress the development of designing of lead compounds with improved bioactivity.

Materials And Methods

Data Collection

The X-ray crystal structure of tubulin protein was obtained from RCSB Protein Data Bank with *PDB ID: 5M7E* (11). We performed the Prepare Protein protocol in Discovery Studio 2.5 (DS2.5) to remove water atoms in crystal structure, repair and optimize side-chain conformation of incomplete amino acids, and protonate the structure of *β*-tubulin protein using Chemistry at HARvard Macromolecular Mechanics (CHARMM) force field (12). The co-crystallized compound, BKM120, in X-ray crystal structure of tubulin protein was employed to define the volume and position of binding site (Fig. 1).

The compounds displayed in Fig. 2 and Table 1 with their cytotoxicity $p\mathrm{GI}_{50}$ values against UACC-62 melanoma cell growth were obtained from previous research in our laboratory (1). All 47 compounds drawn by ChemBioOffice 2010 were prepared by Prepare Ligand protocol in DS2.5 to modify their ionization state to physiological ionization setting.

Table 1
In vitro cytotoxicity pGI_{50} values of compounds against UACC-62 melanoma cell growth.

Compd	R^1	R^2	pGI_{50}
01	-Ph	-	4.62
02	-Ph-4-F	-	6.55
03	-Ph-4-OMe	-	6.12
04	-Ph-3,5-OMe	-	6.82
05	$-CH_2$-Ph-2-F	-	6.48
06	$-CH_2$-Ph-2-F	-H	4.42
07	-Me	$-CH_2CH(CH_3)_2$	4.74
08	-Me	$-C(CH_3)_3$	4.86
09	-Me	$-C(CH_3)_2CH_2CH_3$	4.60
10	-Me	$-CH_2C(CH_3)_3$	4.41
11	-Me	$-CH_2CH_2N(CH_3)_2$	4.98
12	-Me	$-CH_2$-Ph-4-OMe	5.11
13	-Me	$-CH_2$-Ph-4-Cl	5.58
14	-Me	$-CH_2CH_2Cl$	4.70
15	-Ph	-Et	4.70
16	-Ph-4-F	-Et	4.82
17	-Ph-4-OMe	-Et	4.40
18	-Ph-3,5-OMe	-Et	6.45
19	$-(CH_3)_3COOMe$	$-CH_2$-Ph	4.53
20	$-(CH_3)_3COOMe$	-Ph	5.49
21	$-(CH_3)_3COOMe$	-Ph-4-OMe	4.89
22	$-(CH_3)_2COOMe$	-Ph	5.75
23	$-(CH_3)_2COOMe$	$-CH_2$-Ph	4.76

Compd	R^1	R^2	pGI_{50}
24	-$(CH_3)_2$COOMe	-Ph-4-OMe	5.67
25	-Me	-Et	5.31
26	-Me	-$CH(CH_3)CH_2CH_3$	4.55
27	-Me	-$CH_2CH(CH_3)_2$	4.68
28	-Me	-$CH(CH_3)CH_2CH_2CH_3$	5.17
29	-Me	-$CH(CH_2CH_3)_2$	4.99
30	-Me	-$CH_2CH_2CH(CH_3)_2$	4.91
31	-Me	-$CH_2CH(CH_3)CH_2CH_3$	5.00
32	-Me	-$CH_2CH_2N(CH_3)_2$	4.92
33	-Me	-CH_2CH_2OH	4.78
34	-Me	-CH_2-Ph-4-Me	5.95
35	-Me	-CH_2-Ph-4-OMe	5.34
36	-Me	-CH_2-Ph-4-F	5.28
37	-Me	-CH_2-Ph-4-Cl	5.47
38	-Me	-CH_2CH_2Cl	4.89
39	-CH_2Cl	-Et	5.89
40	-Et	-Et	4.54
41	-Pr	-Et	4.59
42	-Ph-3,5-OMe	-Et	4.69
43	-$(CH_3)_3$COOH	-CH_2-Ph	4.76
44	-$(CH_3)_3$COOH	-Ph	4.48
45	-$(CH_3)_3$COOH	-Ph-4-OMe	4.63
46	-$(CH_3)_2$COOH	-CH_2-Ph	4.42
47	-$CH(CH_2CH_3)$-Ph-4-F	-Et	4.95

Molecular Docking Simulation

We performed LigandFit protocol (13) in DS 2.5 to simulate the docking poses of each compound. LigandFit protocol employed Monte-Carlo ligand conformation generation and a shape-based docking, and then it optionally minimized the docking poses with CHARMM force field (12) and filtered out similar docking poses using the clustering algorithm. We consider four different scoring functions, which are -PLP1 (14), -PLP2 (15), –PMF (16), Dock Score, and the interactions between compounds and *β*-tubulin protein to determine the suitable docking pose of each compound. -PLP1, -PLP2, and –PMF are the scoring functions evaluated by summing two types of pairwise interaction, namely hydrogen bonds (H-bonds) and steric interaction, between protein and compound. Dock Score is the scoring function evaluated based on a force field approximation as following equation,

$$\text{Dock Score} = -(\text{ligand\receptor interaction energy} + \text{ligand internal energy})$$

LigPlot^{+} program (17) was performed to generate the 2D ligand-protein interaction diagrams with the H-bond and hydrophobic contacts between compound and *β*-tubulin protein.

Pharmacophore model

For each compounds, we performed FAST generation protocol in DS2.5 to generate their low-energy conformations, and performed 3D-QSAR Pharmacophore Generation protocol in DS2.5 to generate a pharmacophore model using Catalyst HypoGen algorithm (18). Four different pharmacophore features, H-bond donor, H-bond acceptor, hydrophobic, aromatic ring, were considered to construct the common pharmacophore models.

CoMFA and CoMSIA models

SYBYL-X was employed to construct the CoMFA (19) and CoMSIA (20) models. CoMFA was performed with distance-dependent dielectric method to evaluate the steric field descriptors using Lennard–Jones potential energies and electrostatic field descriptors using Coulombic potential energies. CoMSIA was performed with a Gaussian function based on distance to evaluate five physico-chemical properties, which are steric, electrostatic, hydrophobic, H-bond donor, and H-bond acceptor. The partial least-squares regression was performed to obtain the linear correlation between cytotoxicity $p\text{GI}_{50}$ values and descriptors obtained by CoMFA and CoMSIA, respectively.

Results

Molecular Docking Simulation

We defined the structure of *β*-tubulin protein obtained from RCSB Protein Data Bank with *PDB ID: 5M7E* as receptor and defined the volume of co-crystallized compound, BKM120, as binding site (Fig. 1). To validate the accuracy of docking simulation using LigandFit protocol, we performed a docking simulation using LigandFit protocol to redock the co-crystallized compound into the binding site of *β*-tubulin protein. The docking pose of BKM120 is displayed in Fig. 1 with the root-mean-square deviation value of 0.3475

between crystallized structure and docking pose. It represents a suitable docking pose of BKM120 in the docking simulation using LigandFit protocol.

The chemical scaffolds of 47 compounds were displayed in Fig. 2 and Table 1 with their cytotoxicity $p\mathrm{GI}_{50}$ values against UACC-62 melanoma cell growth. The results of docking simulation for 47 compounds listed in Table 2 were determined due to their scoring functions and interactions between each compound and β-tubulin protein. The docking poses of compound **06** and **18** with their interactions illustrated in Fig. 3.

Table 2
The scoring functions of each complex obtained by docking simulation.

Compd	pGI_{50}	Scoring functions			
		-PLP1	-PLP2	-PMF	Dock Score
01	4.62	49.53	42.10	65.64	60.597
02	6.55	53.08	44.26	67.43	64.420
03	6.12	57.21	49.11	73.65	68.265
04	6.82	72.32	66.54	42.76	59.036
05	6.48	60.35	56.63	71.20	54.618
06	4.42	55.34	49.69	66.52	70.679
07*	4.74	82.75	78.22	30.79	64.062
08*	4.86	74.44	70.76	31.42	41.474
09*	4.60	75.86	72.42	30.89	35.540
10*	4.41	75.25	74.41	24.03	56.972
11	4.98	56.15	57.07	26.98	36.577
12*	5.11	82.52	82.36	33.8	72.924
13*	5.58	80.57	78.54	28.38	67.898
14*	4.70	65.15	63.90	19.92	62.934
15*	4.70	86.12	81.85	39.39	66.510
16*	4.82	78.09	76.62	50.23	73.744
17	4.40	71.85	62.26	27.98	67.960
18*	6.45	78.88	74.22	35.13	63.943
19*	4.53	104.54	99.04	60.87	77.695
20*	5.49	95.59	94.47	46.53	75.016
21	4.89	79.29	68.92	37.81	71.057
22*	5.75	94.43	91.27	38.97	75.642
23*	4.76	103.04	98.97	54.89	85.475
24	5.67	79.49	63.82	44.81	73.094
25	5.31	46.74	47.53	55.63	28.806

Compd	pGI_{50}	Scoring functions			
		-PLP1	-PLP2	-PMF	Dock Score
26	4.55	50.91	52.33	59.18	23.133
27	4.68	50.26	52.12	59.73	33.115
28*	5.17	72.41	68.00	24.73	29.004
29	4.99	49.00	49.40	64.54	25.512
30	4.91	54.51	53.43	61.83	32.430
31	5.00	50.43	53.36	63.20	32.907
32	4.92	48.70	48.64	19.61	17.174
33	4.78	46.25	47.45	64.53	44.039
34	5.95	60.37	60.26	71.77	34.015
35	5.34	49.87	58.95	63.83	38.921
36	5.28	77.91	71.98	65.13	41.249
37*	5.47	54.39	50.35	34.90	35.543
38	4.89	51.27	51.43	55.41	33.881
39*	5.89	63.72	62.39	17.04	35.252
40*	4.54	63.22	58.87	22.30	35.720
41*	4.59	68.87	64.09	17.99	35.767
42	4.69	62.66	59.81	72.45	37.338
43	4.76	63.97	60.52	24.98	98.345
44*	4.48	86.80	86.03	47.39	89.869
45*	4.63	91.19	85.55	60.45	91.203
46	4.42	57.89	57.42	26.07	86.964
47	4.95	60.62	65.56	39.74	41.074
*Training set					

Pharmacophore model

In this study, we performed 3D-QSAR Pharmacophore model using 47 compounds to investigate the common pharmacophore features. Figure 4a illustrated the result of the best pharmacophore hypothesis with the distances between each pharmacophore feature. It indicates two H-bond acceptor features, one

aromatic ring feature, and one hydrophobic feature. Figure 4b-c displayed the compounds **06** and **18** mapping in the pharmacophore feature, respectively.

CoMFA and CoMSIA models

The 21 compounds of training set were selected due to their docking poses (Table 2). For alignment of compounds, 21 compounds were superimposed based on their docking poses, and then we constructed the CoMFA and CoMSIA models to determine the correlation between the efficacy of cytotoxicity $p\mathrm{GI}_{50}$ values and the functional groups of compounds. After partial least-squares analysis, the predicted $p\mathrm{GI}_{50}$ values of compounds of training set listed in Table 3 were evaluated by CoMFA model using four components with significantly steric fields (100% contribution) and by CoMSIA model using four components with significantly steric (17.9%), hydrophobic (42.5%), and H-bond donor (39.6%) fields, respectively. The correlations between predicted $p\mathrm{GI}_{50}$ values and experiment $p\mathrm{GI}_{50}$ values for CoMFA and CoMSIA models were displayed in Fig. 5 with the square correlation coefficients (R^2) of 0.857 and 0.817, respectively. The results of CoMFA and CoMSIA models were then illustrated by field contribution maps in Fig. 6 with the high affinity compounds **18**. The favorable and unfavorable regions (85% and 15%, respectively) were evaluated using StDev*coefficients for each field.

Table 3
Experimental pGI_{50} values and predicted pGI_{50} values obtained by CoMFA and CoMSIA models

Compd	pGI_{50}	pGI_{50} (pred.)	
		CoMFA	CoMSIA
7	4.74	4.72	4.71
8	4.86	4.75	4.77
9	4.60	4.76	4.70
10	4.41	4.52	4.36
12	5.11	5.34	5.39
13	5.58	5.44	5.37
14	4.70	4.79	4.79
15	4.70	4.61	4.82
16	4.82	4.84	4.89
18	6.45	6.42	6.41
19	4.53	4.37	4.60
20	5.49	5.49	5.65
22	5.75	5.84	5.78
23	4.76	4.69	4.67
28	5.17	5.18	4.90
37	5.47	5.41	5.48
39	5.89	5.29	5.12
40	4.54	5.10	4.95
41	4.59	4.68	4.85
44	4.48	4.52	4.53
45	4.63	4.53	4.51

Discussion

Molecular Docking Simulation

In docking simulation, these compounds have common H-bond interactions with key residues Lys254 and Lys352. However, the docking poses of compounds **01**–**06** with small R^2 substituent have different docking poses than others. The docking pose of compound **06** illustrated in Fig. 3a-b indicates that the oxygen atoms in 1,4-naphthoquinone moiety and amino fragment of acylamino moiety have H-bonds with key residues Lys254 and Lys352. The docking pose of compound **18** illustrated in Fig. 3c-d indicates that the H-bonds with key residues Lys254 and Lys352 are formed with the oxygen atoms in 1,3-dimethoxybenzene moiety and amino fragment of acylamino moiety. It indicates that compounds with the large alkyl moiety in R^2 substituent have different docking poses. In addition, Fig. 3 indicates that compound **06** also has H-bonds with residues Asn249 using its amine group and has hydrophobic contacts with residues Cys241, Leu248, Asn249, Ala250, Lys254, Leu255, Ala316, and Lys352. For compound **18**, it also has two π-cation interactions with residues Asn258 and Lys352, and it has hydrophobic contacts with residues Gln247, Leu248, Ala250, Lys254, Leu255, Asn258, Met259, Val315, and Lys352. These interactions and hydrophobic contacts supported each compound to bind stabilized in the binding site of *β*-tubulin protein.

Pharmacophore model

For compound **06**, the oxygen atoms in 1,4-naphthoquinone moiety and amino fragment of acylamino moiety were matched with the two H-bond acceptor features in pharmacophore model. For compound **18**, the oxygen atoms in 1,3-dimethoxybenzene moiety and amino fragment of acylamino moiety were matched with the two H-bond acceptor features, phenyl moiety of 1,4-naphthoquinone was matched with the aromatic ring feature, and ethyl group of R^2 substituent was matched with the hydrophobic feature in pharmacophore model. Figure 4 indicates that although the docking poses of compound **06** with small R^2 substituent were differed from the docking pose of compound **18** with large R^2 substituent, they can both fit the pharmacophore features in pharmacophore model and supported the results obtained in docking simulation.

CoMFA and CoMSIA models

In the CoMFA model, Fig. 6a illustrated several favorable steric regions (green) closed to the residues Asn249, Asn258, Val315, Ala354, and several unfavorable steric regions (yellow) closed to the residues Cys241, Ala250, Ala316. Basically, the favorable steric regions are located around the R^1 substituent of compound **18**, and unfavorable steric regions are closed to the terminal of R^2 substituent of compound **18**.

In the CoMSIA model, the favorable and unfavorable regions of steric field displayed in Fig. 6b are similar to CoMFA model, which has favorable regions around the R^1 substituent of compound **18** and unfavorable regions closed to the terminal of R^2 substituent of compound **18**. Figure 6c indicates that there are a favored hydrophobic field (blue) closed to the terminal of R^2 substituent toward the direction of residues Ala316, Lys352 and a disfavored hydrophobic field (white) closed to the terminal of R^1

substituent. Figure 6d introduced the favored (cyan) and disfavored (purple) areas of H-bond donor may further improve the activity.

The results of CoMFA and CoMSIA models indicate that the R^1 substituent of compound **18** preferred to have disfavored hydrophobic fields and have favorable space toward the direction of residue Asn258. In addition, the terminal of R^2 substituent of compound **18** preferred to have hydrophobic substituent toward the direction of residues Ala316 and Lys352, but a long additional chain of substituent would decrease the efficacy of cytotoxicity.

Conclusions

The docking simulation indicates the possible docking poses for all 47 compounds. It also indicates that compounds with large R^2 substituent have different docking poses than compounds with small R^2 substituent. It would explain the reason why most of derivatives cannot maintain the high $p\mathrm{GI}_{50}$ values as the H-bonds between the oxygen atoms in 1,4-naphthoquinone moiety and residues Lys254 or Lys352 may be disrupted. However, some of derivatives such as compound **18** formed the H-bonds with residue Lys254 using the oxygen atoms in R^1 substituent and formed π-cation interactions with residue Lys352 using phenyl moiety of 1,4-naphthoquinone. These interactions and hydrophobic contacts supported these compounds to maintain their binding stabilized in the binding site of *β*-tubulin protein. The results of CoMFA and CoMSIA models indicate that the R^1 substituent of these compounds preferred to have disfavored hydrophobic fields and have favorable space toward the direction of residue Asn258. For R^2 substituent of these compounds, it was preferred to have about 2–3 carbon chain length hydrophobic substituent toward the direction of residues Ala316 and Lys352. These results offer some beneficial advice for further study in development process of designing of lead compounds with improved anticancer bioactivity.

Abbreviations

QSAR, quantitative structure
activity relationship; CoMFA, comparative force field analysis; CoMSIA, comparative similarity indices analysis; DS2.5, Discovery Studio 2.5; CHARMM, Chemistry at HARvard Macromolecular Mechanics; H-bonds, hydrogen bonds;

Declarations

Ethics approval and consent to participate

Not applicable

Consent for publication

Not applicable

Availability of data and materials

All data generated or analyzed during this study are included in this published article

Conflict of Interests

The authors declare no conflict of interest.

Authors' contributions

KCC, CRW and JCL conceived of and designed the experiments, performed the experiments, analyzed the data and wrote the paper.All authors read and approved the final manuscript.

Funding

This research was supported by the Ministry of Science and Technology of Taiwan (MOST 106-2320-B-039-011 and MOST 107-2320-B-039-058,and MOST 108-2320-B-039-044), the China Medical University (CMU107-S-33 and CMU108-MF-70)and the China Medical University Hospital (DMR-108-108 and DMR-108-142).

References

1. Kuo SC,, et al. Synthesis and cytotoxicity of 1,2-disubstituted naphth[2,3-d]imidazole-4,9-diones and related compounds. J Med Chem. 1996;39:1447–51.
2. Gunning PW, Ghoshdastider U, Whitaker S, Popp D, Robinson RC. The evolution of compositionally and functionally distinct actin filaments. J Cell Sci. 2015;128:2009–19.
3. Jordan MA, Wilson L. Microtubules as a target for anticancer drugs. Nat Rev Cancer. 2004;4:253–65.
4. Risinger AL, Giles FJ, Mooberry SL. Microtubule dynamics as a target in oncology. Cancer Treat Rev. 2009;35:255–61.
5. Nami B, Wang Z. (2018) Genetics and Expression Profile of the Tubulin Gene Superfamily in Breast Cancer Subtypes and Its Relation to Taxane Resistance. *Cancers* **10**.
6. Mphahlele MJ, Maluleka MM, Parbhoo N, Malindisa ST. (2018) Synthesis, Evaluation for Cytotoxicity and Molecular Docking Studies of Benzo[c]furan-Chalcones for Potential to Inhibit Tubulin Polymerization and/or EGFR-Tyrosine Kinase Phosphorylation. *Int J Mol Sci* 19.
7. Quan YP,, et al. Molecular modeling study, synthesis and biological evaluation of combretastatin A-4 analogues as anticancer agents and tubulin inhibitors. MedChemComm. 2018;9:316–27.
8. Desbene S, Giorgi-Renault S. Drugs that inhibit tubulin polymerization: the particular case of podophyllotoxin and analogues. Curr Med Chem Anticancer Agents. 2002;2:71–90.
9. Wang Q, et al. (2018) Structural Modification of the 3,4,5-Trimethoxyphenyl Moiety in the Tubulin Inhibitor VERU-111 Leads to Improved Antiproliferative Activities. *J Med Chem*.

10. Mullagiri K, et al. New (3-(1H-benzo[d]imidazol-2-yl))/(3-(3H-imidazo[4,5-b]pyridin-2-yl))-(1H-indol-5-yl)(3,4,5-trimethoxyphenyl)methanone conjugates as tubulin polymerization inhibitors. MedChemComm. 2018;9:275–81.
11. Bohnacker T, et al. Deconvolution of Buparlisib's mechanism of action defines specific PI3K and tubulin inhibitors for therapeutic intervention. Nat Commun. 2017;8:14683.
12. Brooks BR,, et al. CHARMM: A program for macromolecular energy minimization and dynamics calculations. J Comput Chem. 1983;4:187–217.
13. Venkatachalam CM, Jiang X, Oldfield T, Waldman M. LigandFit: a novel method for the shape-directed rapid docking of ligands to protein active sites. J Mol Graph Model. 2003;21:289–307.
14. Gehlhaar DK,, et al. Molecular Recognition of the Inhibitor Ag-1343 by Hiv-1 Protease - Conformationally Flexible Docking by Evolutionary Programming. Chem Biol. 1995;2:317–24.
15. Gehlhaar Daniel K, Bouzida D, Rejto Paul A. (1999) Reduced Dimensionality in Ligand?Protein Structure Prediction: Covalent Inhibitors of Serine Proteases and Design of Site-Directed Combinatorial Libraries. In: *Rational Drug Design.* American Chemical Society, pp. 292–311.
16. Muegge I, Martin YC. A general and fast scoring function for protein-ligand interactions: A simplified potential approach. J Med Chem. 1999;42:791–804.
17. Laskowski RA, Swindells MB. LigPlot+: multiple ligand-protein interaction diagrams for drug discovery. J Chem Inf Model. 2011;51:2778–86.
18. Li H, Sutter J, Hoffman R. (2000) HypoGen: An Automated System for Generating 3D Predictive Pharmacophore Models. In: *Pharmacophore Perception, Development and Use in Drug Design.* Guner O, editor International University Line.
19. Cramer RD, Patterson DE, Bunce JD. Comparative molecular field analysis (CoMFA). 1. Effect of shape on binding of steroids to carrier proteins. J Am Chem Soc. 1988;110:5959–67.
20. Klebe G, Abraham U, Mietzner T. Molecular similarity indices in a comparative analysis (CoMSIA) of drug molecules to correlate and predict their biological activity. J Med Chem. 1994;37:4130–46.

Figures

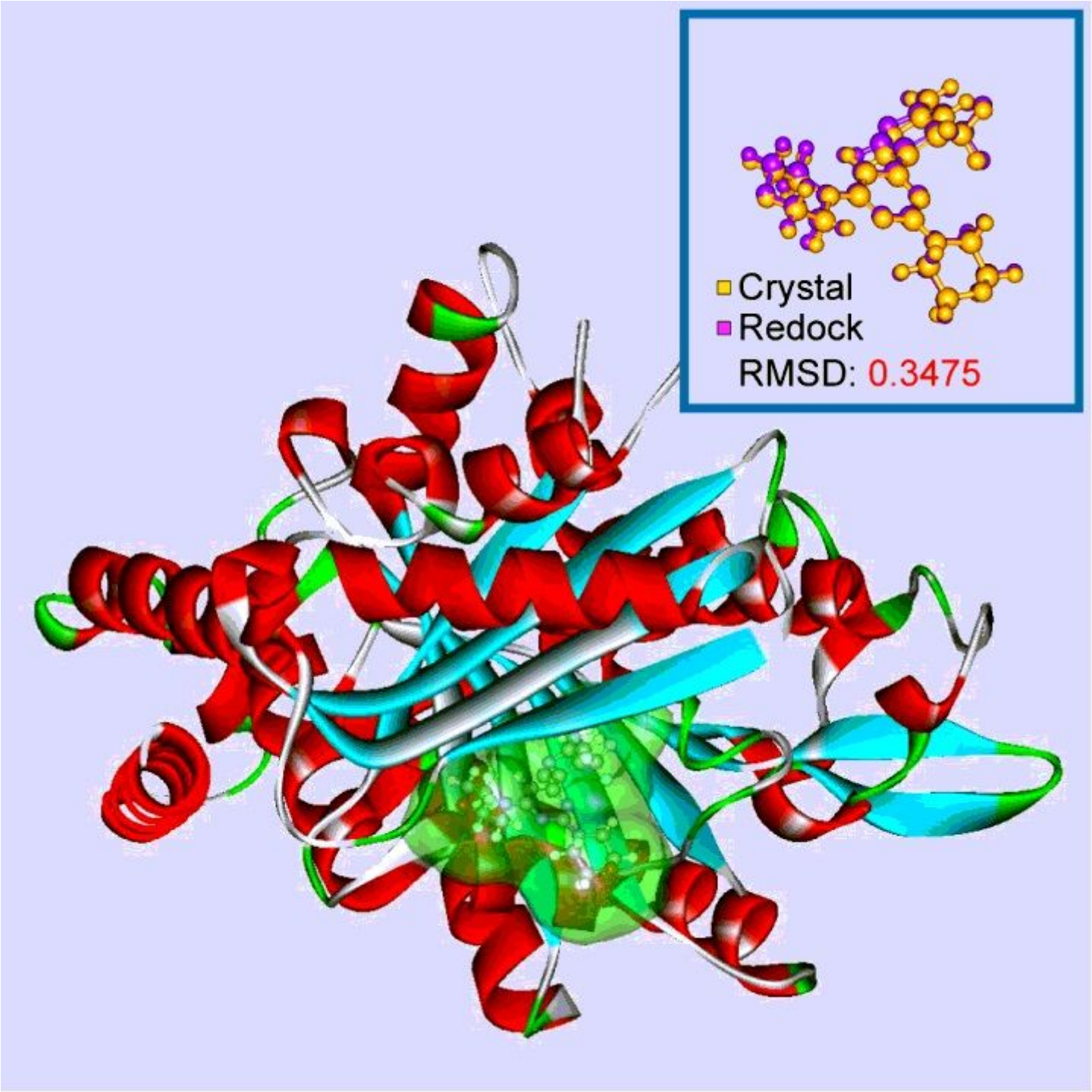

Figure 1

Binding site defined by the volume and position of co-crystallized inhibitor and (upper right) RMSD between crystal structure and molecular docking simulation.

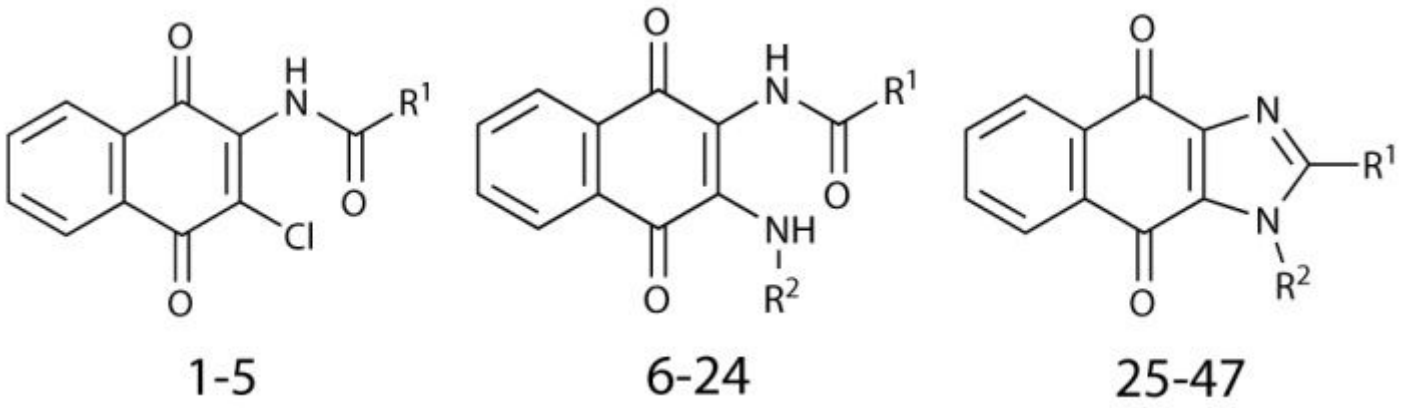

Figure 2

Chemical scaffolds of compounds.

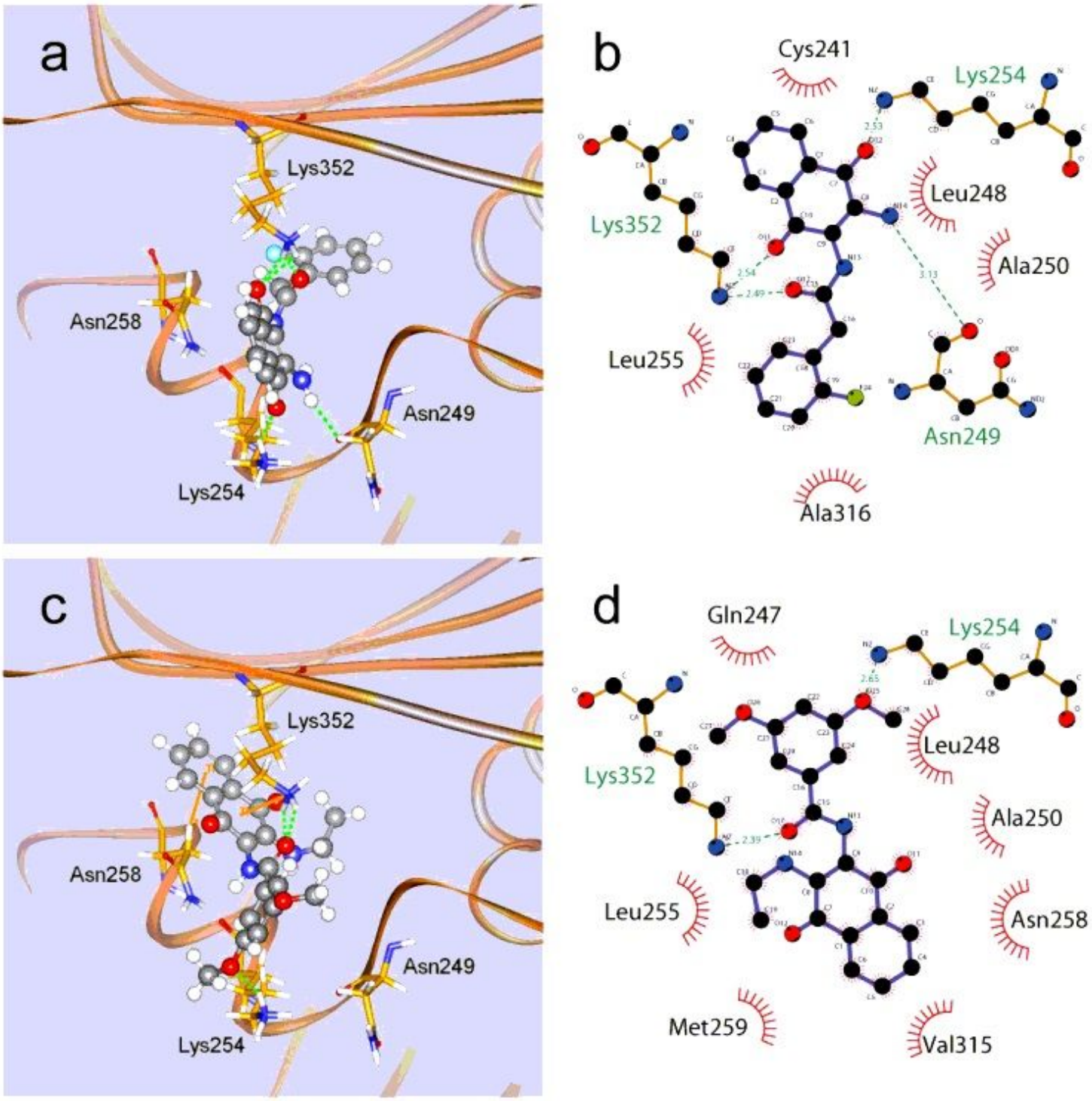

Figure 3

Docking poses of compounds (a)(b) 06 and (c)(d) 18 in binding site ofβ-tubulin protein. (b)(d) drawn by LigPlot+ program.

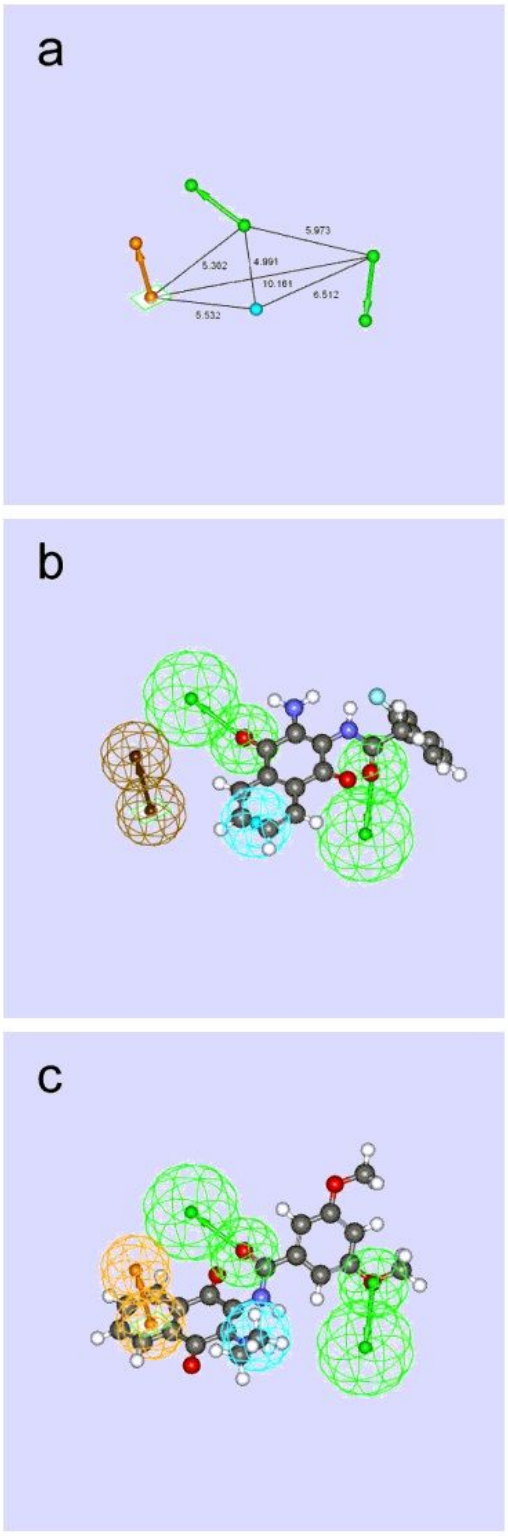

Figure 4

(a) Pharmacophore features mapping with compounds (b) 06 and (c) 18. Hydrogen bond acceptor features illustrated by green lines, hydrophobic feature illustrated by light blue ball, and aromatic ring feature illustrated by orange line.

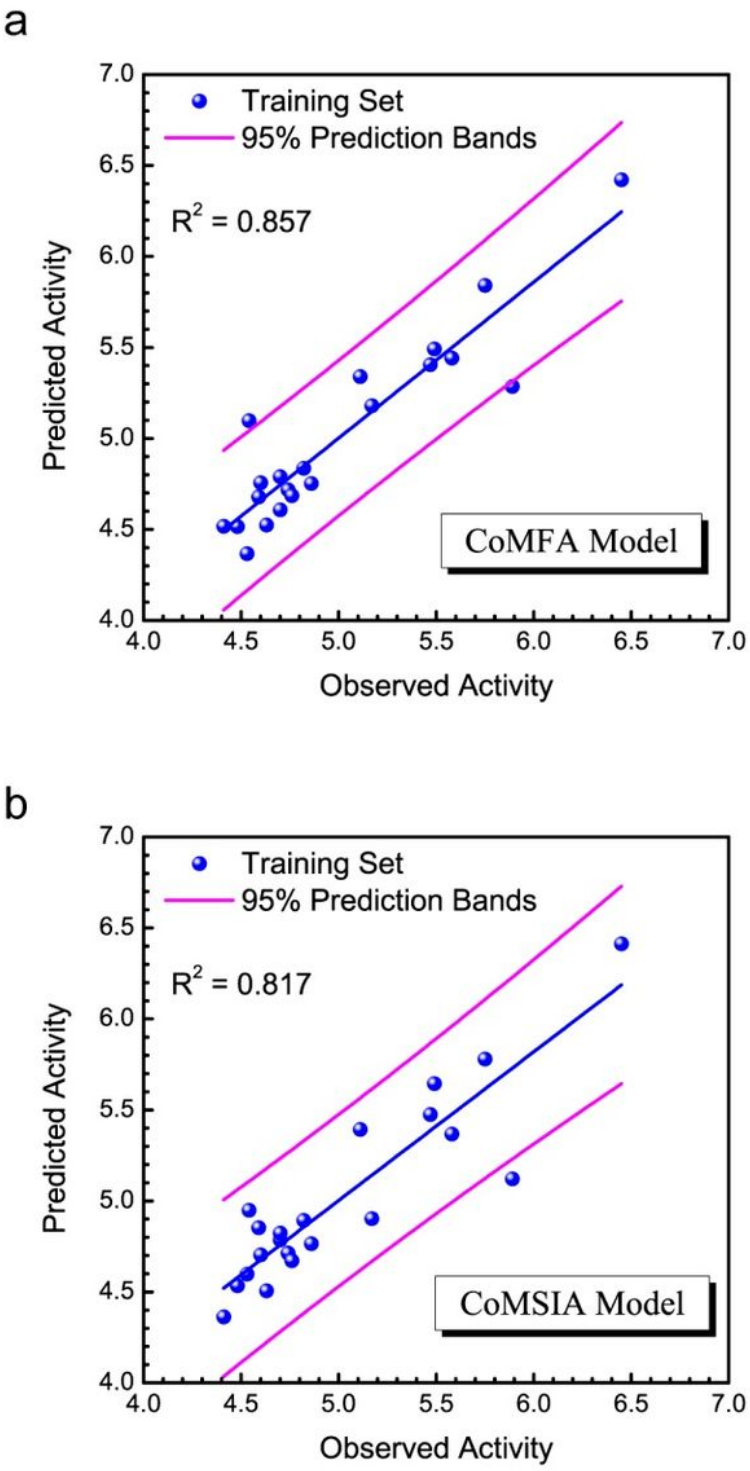

Figure 5

Correlations between predicted pGI50values versus observedpGI50values for (a) CoMFA and (b) CoMSIA models, respectively.

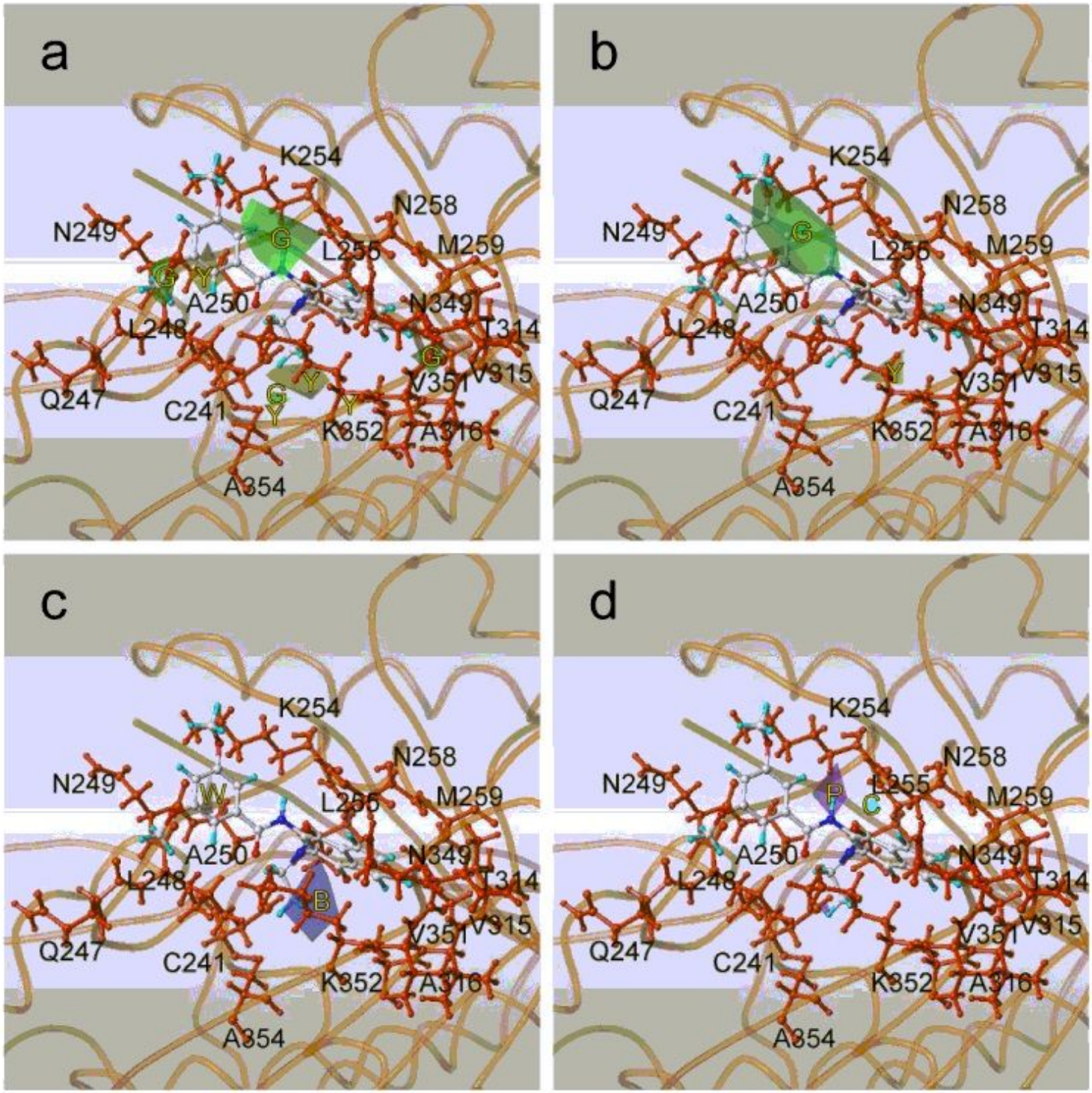

Figure 6

Contour plots illustrating (a) stericproperties revealed by theCoMFA model and (b) steric (c)hydrophobic, (d) hydrogen bond donor properties revealed by theCoMSIA model; Compound 18 shownas templates;B, blue; C, cyan; G, green;W, white; Y, yellow; P, purple.